Article

Hydrocarbon Adsorption in the Flexible Metal Organic Frameworks MIL-53(Al, Cr)

Thuy Khuong Trung, Philippe Trens, Nathalie Tanchoux, Sandrine Bourrelly, Philip L. Llewellyn, Sandra Loera-Serna, Christian Serre, Thierry Loiseau, Franc#ois Fajula, and Ge#rard Fe#rey

J. Am. Chem. Soc., **2008**, 130 (50), 16926-16932 • DOI: 10.1021/ja8039579 • Publication Date (Web): 17 November 2008

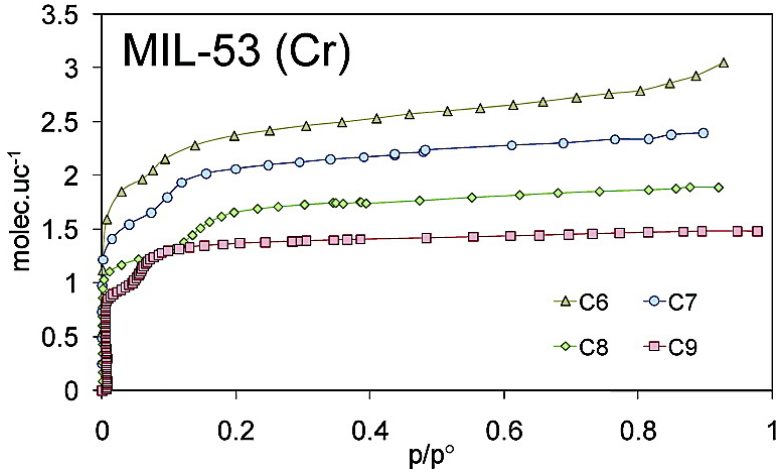

More About This Article

Additional resources and features associated with this article are available within the HTML version:

- Supporting Information
- Access to high resolution figures
- Links to articles and content related to this article
- Copyright permission to reproduce figures and/or text from this article

View the Full Text HTML

J|A|C|S
ARTICLES

Published on Web 11/17/2008

Hydrocarbon Adsorption in the Flexible Metal Organic Frameworks MIL-53(Al, Cr)

Thuy Khuong Trung,[†] Philippe Trens,*[,†] Nathalie Tanchoux,[†] Sandrine Bourrelly,[‡] Philip L. Llewellyn,[‡] Sandra Loera-Serna,[‡] Christian Serre,[§] Thierry Loiseau,[§] François Fajula,[†] and Gérard Férey[§]

MACS, Institut Charles Gerhardt, UMR 5253 CNRS/ENSCM/UM2/UM1, 8 rue de l'Ecole Normale, 34296 Montpellier cedex 5, France, Laboratoire de Chimie de Provence, UMR 6264, CNRS-Université de Provence, Centre de St Jérôme, 13397 Marseille cedex 20, France, and Institut Lavoisier, UMR CNRS 8180, Université Versailles Saint Quentin, 45 avenue des Etats-Unis, 78035 Versailles, France

Received May 27, 2008; Revised Manuscript Received October 27, 2008; E-mail: philippe.trens@enscm.fr

Abstract: A general study of the adsorption of *n*-alkanes in the flexible metal organic framework (MOF) MIL-53 is presented. The roles of the length of the alkyl chain ($n = 1-9$), the nature of the metal (Al, Cr), and temperature were investigated. The shape of the adsorption curves is driven by the alkyl chain length of the *n*-alkanes. While traditional type-I isotherms are observed for short alkanes ($n = 1, 2$), adsorbates with longer chains induce clear substeps in the isotherm curves whose positions depend on the chain length. Such substeps are due to a breathing phenomenon, as proven by ex situ X-ray diffraction analysis. They strongly depend on the amount of adsorbate in the pores and on the nature of the metal (Al, Cr), which, for a given alkane, leads to a strong change in the substep positions despite the similar characteristics of the two metals. The adsorption kinetics are highly sensitive to small variations in temperature. Their detailed analysis in different regions of the isotherms shows in some cases the existence of distinct diffusion regimes and/or conformations within the flexible phases.

Introduction

Metal organic frameworks (MOFs)[1] are a new class of three-dimensional hybrid materials in which organic and inorganic moieties are linked exclusively by strong bonds. Recently, they have attracted much attention because of their potential applications as multifunctional materials in adsorption, storage, separation, ion exchange, optics, magnetism, conductivity, and, more recently, catalysis. Some of them are already produced at the industrial scale.[1−20] Besides the classical strategies used for their synthesis, a more sophisticated method combining targeted chemistry and computational prediction to rationally obtain new crystalline micro- and mesoporous metal carboxylates such as MIL-101 was recently published.[9] Among these new porous materials, the flexible MIL-53(Al, Cr)[16,21] solids are probably some of the most exciting MOFs because of their simple structure and their "breathing" character upon adsorption: previous studies have shown that under CO_2 pressure or in the presence of water (Figure 1),[15,22] the structure of MIL-53(Al, Cr) is able to adjust its cell volume in a reversible manner to

[†] Institut Charles Gerhardt.
[‡] CNRS-Université de Provence.
[§] Université Versailles Saint Quentin.

(1) Férey, G. *Chem. Soc. Rev.* **2008**, *37*, 191.
(2) Férey, G.; Millange, F.; Morcrette, M.; Serre, C.; Doublet, M.-L.; Grenèche, J.-M.; Tarascon, J.-M. *Angew. Chem., Int. Ed.* **2007**, *46*, 3259.
(3) Moulton, B.; Zaworotko, M. J. *Chem. Rev.* **2001**, *101*, 1629.
(4) Xiong, R. G.; You, X. Z.; Abrahams, B. F.; Xue, Z.; Che, C. M. *Angew. Chem., Int. Ed.* **2001**, *40*, 4422.
(5) Zhao, X.; Xiao, B.; Fletcher, A. J.; Thomas, K. M.; Bradshaw, D.; Rosseinsky, M. J. *Science* **2004**, *306*, 1012.
(6) Ockwig, N. W.; Delgado-Friederichs, O.; O'Keeffe, M.; Yaghi, O. M. *Acc. Chem. Res.* **2005**, *38*, 176.
(7) Denayer, J. F. M.; De Meyer, K.; Martens, J. A.; Baron, G. V. *Angew. Chem. Int. Ed.* **2003**, *42*, 2774.
(8) Matsuda, R.; Kitaura, R.; Kitagawa, S.; Kubota, Y.; Belosludov, R. V.; Kobayashi, T. C.; Sakamoto, H.; Chiba, T.; Takata, M.; Kawazoe, Y.; Mita, Y. *Nature* **2005**, *436*, 238.
(9) Férey, G.; Mellot-Draznieks, C.; Serre, C.; Millange, F. *Acc. Chem. Res.* **2005**, *38*, 217.
(10) Zeng, M. H.; Wang, B.; Wang, X. Y.; Zhang, W. X.; Chen, X. M.; Gao, S. *Inorg. Chem.* **2006**, *45*, 7069.
(11) Rosi, N.; Eckert, J.; Eddaoudi, M.; Vodak, D.; Kim, J.; O'Keeffe, M.; Yaghi, O. *Science* **2003**, *300*, 1127.
(12) Müller, U.; Schubert, M.; Teich, F.; Pütter, H.; Schierle-Arndt, K.; Pastré, J. *J. Mater. Chem.* **2006**, *16*, 626.
(13) Taylor, T. J.; Bakhmutov, V. I.; Gabbaï, F. P. *Angew. Chem., Int. Ed.* **2006**, *45*, 7030.
(14) Alaerts, L.; Kirschhock, C. E.; Maes, M.; van der Veen, M. A.; Finsy, V.; Depla, A.; Martens, J. A.; Baron, G. V.; Jacobs, P. A.; Denayer, J. F. M.; De Vos, D. E. *Angew. Chem., Int. Ed.* **2007**, *46*, 4293.
(15) Férey, G.; Latroche, M.; Serre, C.; Millange, F.; Loiseau, T.; Percheron-Guegan, A. *Chem. Commun.* **2003**, 2976.
(16) Loiseau, T.; Serre, C.; Huguenard, C.; Fink, G.; Taulelle, F.; Henry, M.; Bataille, T.; Férey, G. *Chem.—Eur. J.* **2004**, *10*, 137.
(17) Kitaura, R.; Seki, K.; Akiyama, G.; Kitagawa, S. *Angew. Chem., Int. Ed.* **2003**, *42*, 428.
(18) Rowsell, J. L. C.; Yaghi, O. M. *Angew. Chem., Int. Ed.* **2005**, *44*, 4670.
(19) Kitagawa, S.; Kitaura, R.; Noro, S.-I. *Angew. Chem., Int. Ed.* **2004**, *43*, 2334.
(20) Llewellyn, P. L.; Bourrelly, S.; Serre, C.; Filinchuk, Y.; Férey, G. *Angew. Chem., Int. Ed.* **2006**, *45*, 7751.
(21) Serre, C.; Millange, F.; Noguès, M.; Thouvenot, C.; Marsolier, G.; Louër, D.; Férey, G. *J. Am. Chem. Soc.* **2002**, *124*, 13519.
(22) Bourrelly, S.; Llewellyn, P. L.; Serre, C.; Millange, F.; Loiseau, T.; Férey, G. *J. Am. Chem. Soc.* **2005**, *127*, 13519.

10.1021/ja8039579 CCC: $40.75

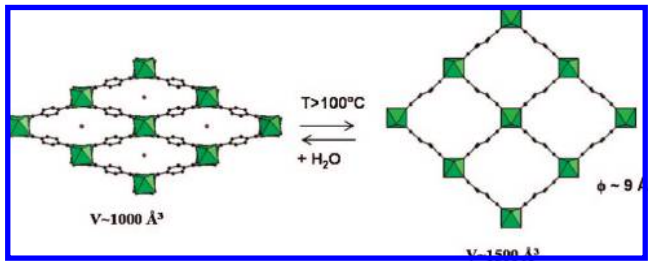

Figure 1. Schematic view of the breathing phenomenon of MIL-53(Al, Cr) (view along the *c* axis) upon adsorption/desorption of water.

optimize interactions between the guest molecules and the framework, with no evidence of bond breaking.

To date, most reports concern the adsorption of gases, while vapor studies are still scarce, with only a few results dealing with the adsorption of alkanes.[23−25] Recently, MOFs proved their efficiency in the chromatographic separation of alkanes (linear or branched), with *n*-hexane separated from *n*-pentane and, more interestingly, methylbutane from *n*-pentane.[26]

However, the mechanisms of separation have not been completely elucidated,[27] and much effort must still be spent on the adsorption of model molecules in MOFs. The influence of flexibility on the adsorption of nonpolar vapors in MOFs has not been investigated to date, and this would be of great interest in order to determine whether or not adsorption might lead to unusual breathing phenomena. This study relates the adsorption of vapors of linear *n*-alkanes ($n = 1-9$) in the MIL-53(Al, Cr) hybrid materials[21] in terms of adsorption capability, influence of temperature, kinetics of adsorption, and sorbate/sorbent interactions.

Experimental Section

Synthesis. The preparation of MIL-53(Al, Cr)$_{as}$ (where the *as* subscript stands for as-synthesized) was previously reported.[15,16] While the removal of the free acid from the pores can be performed by calcination, another activation route has been developed to avoid formation of the metal oxide byproduct. MIL-53(Al, Cr)$_{as}$ was treated under solvothermal conditions in dimethylformamide (DMF) at 150 °C overnight. Typically, 1 g of MIL-53$_{as}$ was dispersed in 25 mL of DMF and introduced into a Teflon-lined steel autoclave for 15 h at 150 °C. The product was cooled, filtered, and calcined overnight at 200 °C (Cr) or 280 °C (Al) in air. The solid readsorbs water at room temperature to give low-temperature MIL-53, or $M^{III}(OH)\{O_2C-C_6H_4-CO_2\}\cdot H_2O$ (M = Cr, Al). The usual characterization experiments (powder XRD, TGA, IR spectroscopy, BET analysis) were performed on the MIL-53(Al, Cr) phases to confirm their purity.

C1−C4 Hydrocarbon Adsorption. The adsorption experiments were carried out at 303 K at pressures up to 50 bar on a laboratory-made gas dosing system connected to a commercial gravimetric measuring system (Rubotherm Präzisionsmesstechnik GmbH). The balance itself has a sensitivity of 10 μg and a resolution of 0.01 mg. An advantage of this system is the incorporation of a titanium sinker that, when weighted, allows a direct measurement of the buoyancy effect and its correction to the adsorbed amounts. A step-by-step mode of gas introduction was used here, requiring the criterion of negligible weight change (<80 μg over 15 min) to be met before introduction of the following dose. Prior to each experiment, the sample was outgassed at 250 °C for 16 h. A typical adsorption experiment usually takes ~24 h, but in many cases in this study, some points required more than 7 days to reach adsorption equilibrium.

C5−C9 Hydrocarbon Adsorption. Adsorption/desorption experiments on the C5−C9 hydrocarbons were performed with a homemade apparatus previously described.[28,29] This setup is based on manometric measurements [with two capacitative pressure gauges (0−10 and 0−1000 mbar)]. The sample cell can be disconnected from the system to undergo a prior outgassing at temperatures up to 250 °C under a vacuum of 10^{-3} mbar. *n*-Alkanes used as adsorbates (provided by Aldrich, purity >99.9%) were outgassed and stored over activated 3 Å molecular sieve.

Powder X-ray Diffraction. To understand the C6 and C9 adsorption, high-resolution powder X-ray diffraction (XRD) patterns of MIL-53(Al) products were collected either on a D8 Bruker diffractometer with monochromatized Cu Kα_1 radiation using a rotating sample holder or at the Swiss−Norwegian synchrotron beamline BM01A at the European Synchrotron Radiation Facility (ESRF, Grenoble, France). The MIL-53(Al) powdered samples were introduced into quartz capillaries ($\varnothing$ = 0.7 mm), which were attached to a manifold system allowing vacuum, heat treatment, and vapor dosing. The samples were thus outgassed under a vacuum below 10^{-2} mbar and heated to 200 °C for 2 h. The manifold was then placed in a temperature-controlled room at 24 °C, and the sample was maintained at 20 °C in a liquid thermostat. This temperature was chosen as it is the same as the one from the XRD chamber. *n*-Hexane and *n*-nonane were previously distilled, and 5A zeolite pellets were put into the liquid to adsorb traces of water and other impurities. The dosing was carried out by keeping the liquid at the appropriate temperature in a second liquid cryostat to ensure that the required relative pressure was maintained with respect to the sample temperature. The pressure was checked using a pressure gauge. Once both the sample and liquid were at the appropriate temperature, the two were connected, and an equilibrium time of 1 h was used. For hexane adsorption, temperatures of −14.5 and +8 °C ensured relative pressures of 0.17 and 0.59, respectively. In the case of *n*-nonane adsorption, temperatures of −12 and +12 °C ensured relative pressures of 0.10 and 0.60, respectively. After equilibrium, the capillary was flame-sealed prior to measurement of the diffraction patterns.

The cell parameters of the various forms of MIL-53(Al) were deduced from the XRD patterns using the Dicvol software.[30] Pattern matching of the different hexane- or nonane-loaded MIL-53(Al) forms was performed with the corresponding XRD patterns and Fullprof.2k using the WinPLOTR software package.[31]

In a second step, a series of in situ synchrotron powder diffraction experiments were carried out at the Swiss−Norwegian Beamlines (SNBL) at ESRF. The data were collected on 1.0 mm quartz capillaries filled with the sample using a MAR345 imaging plate at a sample-to-detector distance of 300 mm with λ = 0.7 Å. The sample was cooled to 100 K using a cryostream and then heated back to 300 K. The data were integrated using the Fit2D program (Dr. A. Hammersley, ESRF) and a calibration measurement of a NIST LaB_6 standard sample. Uncertainties in the integrated intensities were calculated at each 2θ point by applying Bayesian

(23) Chen, B.; Liang, C.; Yang, J.; Contreras, D. S.; Clancy, Y. L.; Lobkovsky, E. B.; Yaghi, O. M.; Dai, S. *Angew. Chem., Int. Ed.* **2006**, *45*, 1390.
(24) Pan, L.; Olson, D. H.; Ciemnolonski, L. R.; Heddy, R.; Li, J. *Angew. Chem., Int. Ed.* **2006**, *45*, 616.
(25) Stallmach, F.; Groger, S.; Kunzel, V.; Karger, J.; Yaghi, O. M.; Hesse, M.; Müller, U. *Angew. Chem., Int. Ed.* **2006**, *45*, 2123.
(26) Finsy, V.; De Bruyne, S.; Alaerts, L.; De Vos, D.; Jacobs, P. A.; Baron, G. V.; Denayer, J. F. M. *Stud. Surf. Sci. Catal.* **2007**, *170*, 2048.
(27) Uemura, K.; Yamasaki, Y.; Komagawa, Y.; Tanaka, K.; Kita, H. *Angew. Chem., Int. Ed.* **2007**, *46*, 6662.
(28) Trens, P.; Tanchoux, N.; Papineschi, P.-M.; Maldonado, D.; di Renzo, F.; Fajula, F. *Microporous Mesoporous Mater.* **2005**, *86*, 354.
(29) Trens, P.; Tanchoux, N.; Maldonado, D.; Galarneau, A.; Di Renzo, F.; Fajula, F. *New J. Chem.* **2004**, *28*, 874–879.
(30) Boultif, A.; Louër, D. *J. Appl. Crystallogr.* **1991**, *24*, 987–993.
(31) (a) Rodriguez-Carvajal, J. In *Collected Abstracts of Powder Diffraction Meeting*; Toulouse, France, 1990; p 127. (b) Roisnel, T.; Rodriguez-Carvajal, J. In *Abstracts of the Seventh European Powder Diffraction Conference*; Barcelona, Spain, 2000; p 71.

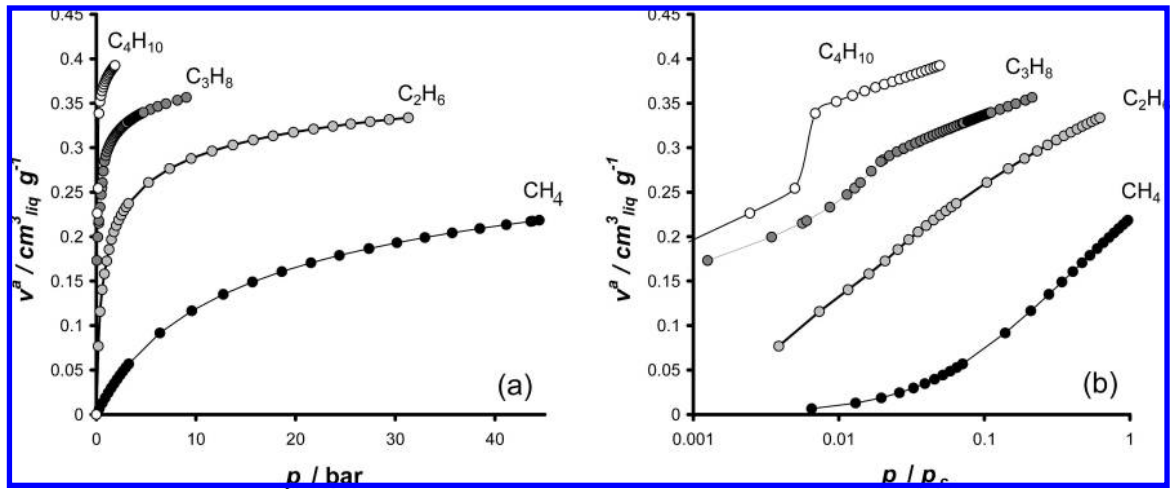

Figure 2. Isotherms of C1−C4 *n*-alkanes on MIL-53(Cr) at 303 K, showing volume adsorbed as a function of (a) pressure and (b) $\log(p/p_c)$.

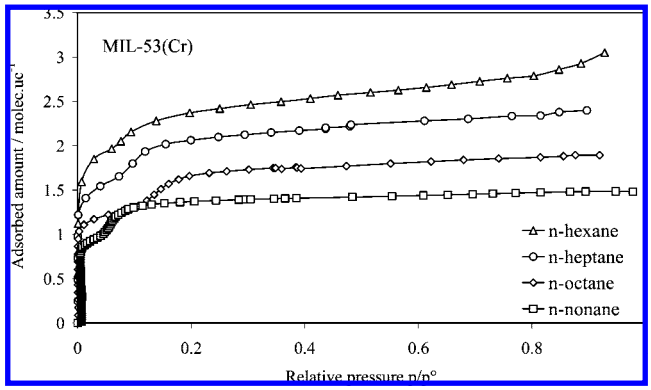

Figure 3. Adsorption of *n*-alkanes onto MIL-53(Cr) at 313 K: (△) *n*-hexane, (○) *n*-heptane, (◇) *n*-octane, (□) n-nonane.

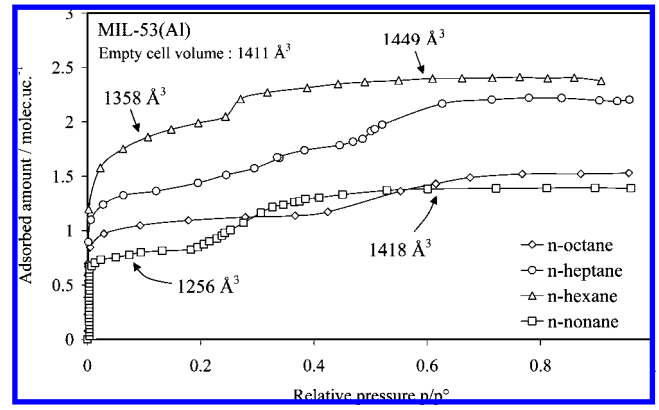

Figure 4. Adsorption of *n*-alkanes onto MIL-53(Al) at 313 K: (△) *n*-hexane, (○) *n*-heptane, (◇) *n*-octane, (□) n-nonane. Numerical values indicate the cell volumes at the onset of the plateaus.

statistics to the intensity data while considering the geometry of the detector (Add Sigmas program, Dr. Y. Filinchuk, SNBL).

Results and Discussion

Adsorption Isotherms of *n*-Alkanes over MIL-53(Cr). The short-chain hydrocarbon adsorption isotherms are given in Figure 2. If at first glance it appears that Langmuir isotherms are obtained (Figure 2a), closer observation using a semilogarithmic scale highlights the existence of substeps in the isotherms for the C3 and C4 hydrocarbons. These substeps are far more systematic in the C5−C9 hydrocarbon isotherms (Figures 3 and 4). The strong uptakes obtained at low pressures indicate the presence of strong host−guest interactions through confinement effects. *n*-Alkanes usually do not exhibit any particular interaction with mineral oxides, but here (see below), even though *n*-alkane polarizabilities are known to be quite weak, it is likely that interactions with both the organic and inorganic parts of the MOF occur, in agreement with preliminary molecular simulation studies.[32] The position of the step is a function of pressure and could be used for a pressure- or vacuum-swing adsorption process for separation of the hydrocarbons.

Examination of the amounts adsorbed shows that they compare favorably to those observed in various zeolitic materials. In terms of adsorption capabilities, MIL-53(Al, Cr) adsorbs 50% more than zeolites.[33]

These substeps indicate a two-step adsorption mechanism, which could originate either from successive adsorptions by inorganic and organic sites or from breathing and its correlative variations in cell volume at invariant topology, as already observed for water and carbon dioxide.

Ex situ high-resolution XRD analyses were therefore performed on *n*-hexane- and *n*-nonane-loaded MIL-53(Al) samples at the relative pressures corresponding to the various plateaus ($p/p° \approx 0.1-0.2$ and 0.6) (Figure 5). For hexane, at low pressure ($p/p° \approx 0.17$), the XRD pattern was indexed in an orthorhombic cell [a = 17.3(2) Å, b = 11.79(2) Å, c = 6.63(1) Å, space group *Imcm*] with a cell volume of 1358.2(2) Å^3, which is clearly smaller than the volume of 1411 Å^3 for the dried solid.[5] At a higher relative pressure ($p/p° \approx 0.6$), the cell volume increases to 1449.0(2) Å^3 [a = 16.24(2) Å, b = 13.47(2) Å, c = 6.62(1) Å, space group *Imcm*], which is in agreement with an increase in adsorbed volume between the two plateau regions. This corresponds to a breathing magnitude of ∼7% between the low- and high-pressure forms.

A larger breathing magnitude (∼13%) is observed with *n*-nonane [for the low-pressure form ($p/p° \approx 0.11$), a = 18.10(2),

(32) Nicholson, T. M.; Bhatia, S. K. *J. Phys. Chem. B.* **2006**, *110*, 24834.

(33) Chen, C. Y.; Zones, S. I. *Stud. Surf. Sci. Catal.* **2001**, *135*, 222.

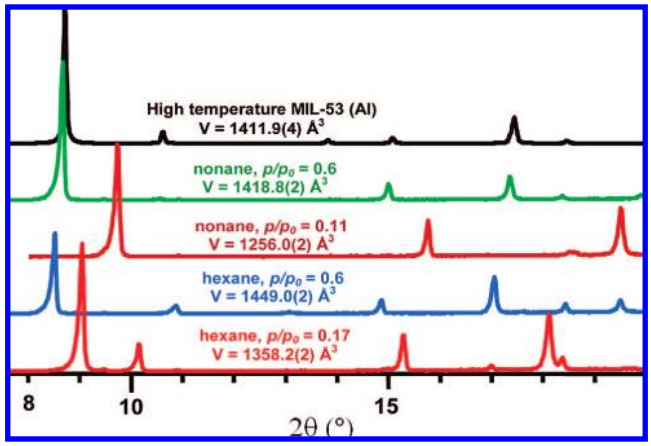

Figure 5. XRD patterns (monochromatic copper radiation) of MIL-53(Al) loaded with various amounts of adsorbed *n*-hexane or *n*-nonane, with relative pressures $p/p°$ and calculated cell volumes V as indicated: (red) *n*-hexane, $p/p° = 0.17$, $V = 1358.2$ Å^3; (blue) *n*-hexane, $p/p° = 0.60$, $V = 1449$ Å^3; (purple) *n*-nonane, $p/p° = 0.11$, $V = 1256.0$ Å^3; (green) *n*-nonane, $p/p° = 0.6$, $V = 1418.8$ Å^3; (black) MIL-53(Al) without alkane at high temperature.

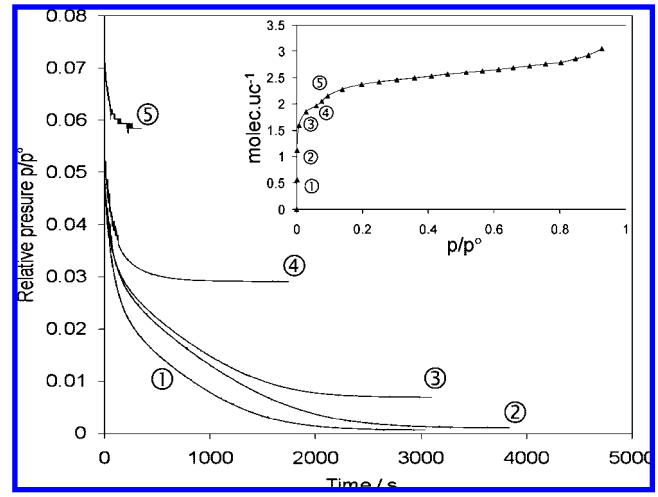

Figure 6. Kinetics of adsorption of *n*-hexane over MIL-53(Cr) at 313 K. The adsorption isotherm is recalled in the inset. The vertical axis represents the relative pressure measured as adsorption onto the sample occurs. Circled numbers indicate the adsorption domains described in the text.

$b = 10.48(2)$, $c = 6.62(1)$ Å, and $V = 1256.0(2)$ Å^3; for the high-pressure form ($p/p° \approx 0.6$), $a = 16.71(2)$, $b = 12.83(2)$, $c = 6.62(1)$ Å, and $V = 1418.8(2)$ Å^3; space group *Imcm* in both cases). At low pressure, the percentage of the total amount of adsorbed alkane is larger for C6 (85%) than for C9 (60%), and therefore, the shrinkage of the structure is more pronounced for C9 than for C6. The sorption isotherm reflects the simultaneous influence of the intensities of the various host−guest interactions and their size effects on the extent of breathing.

From the above results, *n*-hexane and *n*-nonane lead to some swelling of the framework. The sorption isotherms obtained in the case of *n*-heptane and *n*-octane indicate that the same swelling process can occur. *n*-Methane does not lead to swelling.[34] It can simply be mentioned here that this relates to a threshold in the adsorption enthalpy (−20 kJ mol^{-1}) above which breathing occurs. A linear increase in the heat of adsorption of alkanes with increasing alkyl chain length (∼10 kJ mol^{-1} per additional carbon atom in the chain) is expected, as for zeolites.[13]

Within the MIL-53 topology, the dynamic effects associated with flexibility spectacularly depend on the nature of the metal. Whereas the MIL-53(Al, Cr) evacuated solids exhibit the open form, dehydrated MIL-53(Fe, Ga) corresponds to the shrunk variety.[35] Even within the (Al, Cr) subclass, the responses to the alkane stimulus are different. The substeps are shifted to higher relative pressure when chromium is replaced by aluminum and in going from *n*-butane to *n*-octane, even though there is some ambiguity in the case of MIL53(Al)/*n*-heptane due to the occurrence of several minor substeps. The MIL-53(Cr) substeps systematically appear at lower relative pressures than those in MIL-53(Al) (Figures 3 and 4), indicating that specific alkane−metal interactions with various energies exist in this topology.

n-Nonane does not follow the above trend, however: the adsorption substep appears at a much lower relative pressure. No definitive explanation for this behavior can be given, but several effects could induce it (host−guest structural commensurability, entropic effects, conformation due to confinement, etc.). Furthermore, it is worthy of note that the adsorption substep is shifted to lower relative pressures regardless of the metal concerned.[36]

Influence of Pore Filling on Kinetics of Adsorption. Preliminary experiments were performed to make sure that vapor diffusion into the sample cell was not the limiting stage of the overall adsorption process. Nitrogen gas was therefore introduced into the sample cell at the adsorption temperature of 313 K, and pressure equilibrium was reached within a few seconds. From this standpoint, the kinetics of adsorption of *n*-alkane vapors over MIL-53(Cr) materials was determined for each adsorption equilibrium. A given amount of vapor was introduced into the sample cell, in which pressure was measured by a pressure gauge. The setup has already been detailed in a previous paper.[28] Equilibration was considered to be obtained when the variation of pressure was not detectable (typically less than 10^{-4} torr/min). Similar results (not shown) were obtained when MIL-53(Al) was used.

On the basis of the adsorption curves, different stages can be distinguished that could induce differences in adsorption kinetics. Five typical adsorption domains were investigated: (1) the very first stages of the adsorption, (2) further sorption in the initial stages of the adsorption, (3) the knee of the adsorption isotherm, (4) the intermediate region before the substep, and (5) the saturation plateau, as exemplified in Figure 6 for *n*-hexane.

After the introduction of each dose, the time needed to reach equilibrium was measured for each *n*-alkane. During the very first stages of adsorption, the length of the alkyl chain clearly influences both the time to equilibrium (which increases in going from from C7 to C9) and the adsorption process. Hexane presents a special behavior.

Indeed, nonane [as well as pentane, heptane, and octane (not shown)] follows a simple exponential decay, as shown by the

(34) Llewellyn, P. L.; Maurin, G.; Devic, T.; Loera-Serna, S.; Rosenbach, N.; Serre, C.; Bourrelly, S.; Horcajada, P.; Filinchuk, Y.; Férey, G. *J. Am. Chem. Soc.* **2008**, *130*, 12808.
(35) Millange, F.; Guillou, N.; Walton, R. I.; Grenèche, J.-M.; Margiolaki, I.; Férey, G. *Chem. Commun.* **2008**, 4732.
(36) Pellenq, N.; Llewellyn, P. L.; Grillet, Y.; Rouquerol, J. *J. Therm. Anal.* **1994**, *41*, 1343.

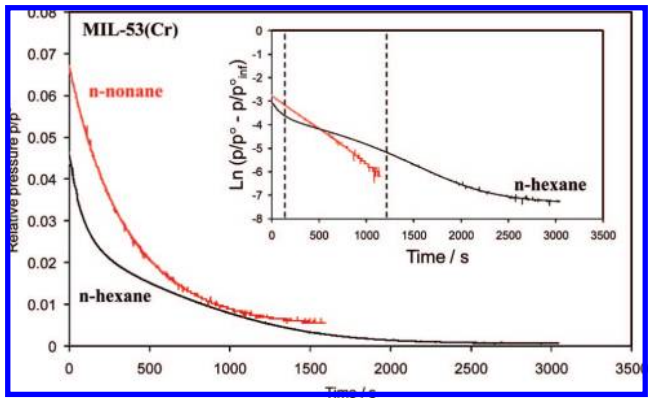

Figure 7. Kinetics of adsorption of *n*-hexane (solid line) and *n*-nonane (dashed line) over MIL-53(Cr) at 313 K during the very first adsorption stages. The vertical axis represents the relative pressure measured as adsorption onto the sample occurs. Inset: corresponding plots of ln-$[(p/p^\circ) - (p/p^\circ)_{eq}]$ vs time.

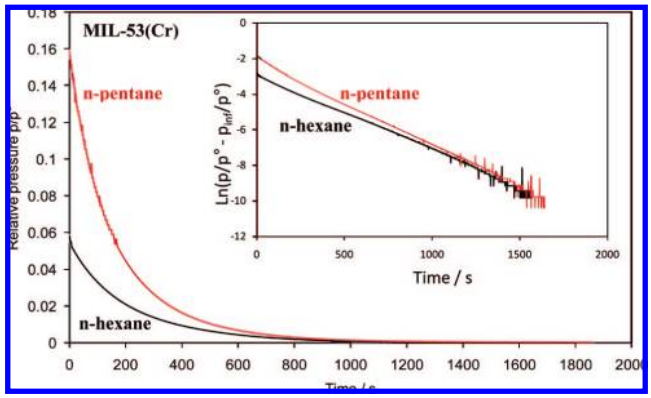

Figure 8. Kinetics of adsorption of (black) *n*-hexane and (red) *n*-pentane over MIL-53(Cr) at 303 K. The vertical axis represents the relative pressure measured in the sample cell as adsorption onto the sample occurs. Inset: corresponding plots of $\ln[(p/p^\circ) - (p/p^\circ)_{eq}]$ vs time.

linear relationship between $\ln[(p/p^\circ) - (p/p^\circ)_{eq}]$ and time (inset of Figure 7). This linearity suggests that the adsorption follows a single process.

The curve obtained for *n*-hexane is far more complex. Three regions can be distinguished at 313 K for the short alkyl chain length, suggesting that tiny differences in the sorbate/sorbent interaction are sufficient to strongly modify the adsorption kinetics.

Moreover, it is also interesting to note that the equilibration time is longer for *n*-hexane than for the other sorbates (Figure S1 in the Supporting Information). The specific case of *n*-hexane seems to suggest that diffusion is probably not the limiting mechanism during the adsorption process, as bulkier *n*-alkanes adsorbed in the same materials led to faster kinetics of adsorption. If it were the case, this might be due to a particular interaction between *n*-hexane species in a specific conformation and the flexible skeleton.

Influence of Temperature on the Kinetics of Adsorption and the Adsorbed Amounts at Saturation. The host−guest interaction balance can also be modified by a slight change in the temperature. While three successive regimes for adsorption of *n*-hexane at 313 K were observed, a temperature decrease of only 10 K made them disappear (Figure 8). This suggests a drastic temperature dependence of (i) the diffusion coefficients and (ii) the extent of breathing. The equilibrium times and

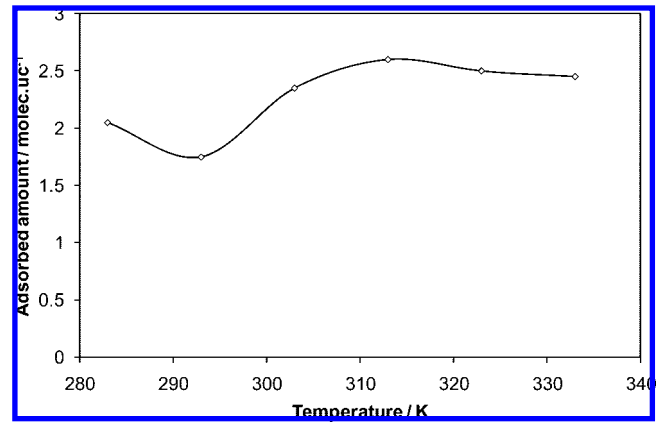

Figure 9. Amounts of *n*-hexane adsorbed on MIL-53(Cr) at $p/p^\circ = 0.4$ as a function of temperature.

behavior of C6 became very close to those of C5 as well as to those of C7−C9 (not shown).

The overall adsorbed amounts of sorbate should decrease when temperature increases. However, plotting the data obtained at saturation of the *n*-hexane sorption isotherms over MIL-53(Cr) yielded a different evolution (Figure 9). This unusual thermal evolution of the adsorption capacity of *n*-hexane does not mean at all that the system is in conflict with thermodynamics. Indeed, this peculiar feature also takes into account the flexibility of the framework. Recently, a study of the highly flexible MIL-88 hybrid solids showed that the magnitude of their pore openings upon adsorption of liquids increased with temperature.[37] Thus, we suggest here that the present complex behavior might due to a competition between two distinct phenomena: (i) an increase in the pore opening of the MIL-53 solids with temperature and (ii) in agreement with thermodynamics, a decrease in the adsorbed amount with increasing temperature. At lower temperatures (283−293 K), the second mechanism prevails, and a decrease in the sorption capacity is observed. When the temperature is increased to 313 K, one part of the heat contributes to the opening of the structure and therefore to an increase in the capacity at saturation. Above 313 K, because of the geometric limitations, the maximum pore opening of MIL-53 is probably reached, and a decrease of the loading capacity with increasing temperature is observed, as for a rigid phase. It can be concluded that in the case of *n*-hexane, the chemical potential of the gas phase (which is directly related to temperature) may be employed to control the pore breathing.

An alternative explanation could be that the adsorption processes are activated upon an increase in temperature to overcome diffusion limitations, especially in the case where micropores have to accommodate guest species in relation with structural breathing effects. This activation-related behavior has often been observed in the literature in the case of the adsorption of vapors in zeolites.[38]

To further analyze the unusual evolution of the maximum adsorption capacity of MIL-53 as a function of the temperature,

(37) (a) Serre, C.; Mellot-Draznieks, C.; Surblé, S.; Audebrand, N.; Filinchuk, Y.; Férey, G. *Science* **2007**, *315*, 1828. (b) Liu, Y.; Her, J.-H.; Dailly, A.; Ramirez-Cuesta, A. J.; Neumann, D. A.; Brown, C. M. *J. Am. Chem. Soc.* **2008**, *130*, 11813.

(38) Derouane, E. G.; André, J. M.; Lucas, A. A. *J. Catal.* **1988**, *110*, 58.

Table 1. Cell Parameters as a Function of Temperature[a]

T (K)	*a* (Å)	*b* (Å)	*c* (Å)	*β* (deg)	space group	cell volume (Å^3)
300	16.22(1)	13.53(1)	6.63(1)	–	*Pnam* (No. 62)	1455(1)
280	16.02(1)	13.78(1)	6.63(1)	–	*Pnam* (No. 62)	1464(1)
260	15.7(1)	14.17(1)	6.64(1)	–	*Pnam* (No. 62)	1476(1)
240	15.33(1)	14.58(1)	6.6(1)	–	*Pnam* (No. 62)	1482(1)
220	15.35(1)	14.61(1)	6.63(1)	–	*Pnam* (No. 62)	1488(1)
200	15.36(1)	14.60(1)	6.62(1)	–	*Pnam* (No. 62)	1484(1)
180	15.37(1)	14.57(1)	6.62(1)	–	*Pnam* (No. 62)	1484(1)
160	15.40(1)	14.55(1)	6.62(1)	–	*Pnam* (No. 62)	1483(1)
160	*17.55(2)*	*12.09(2)*	*6.65(2)*	*105.2(2)*	*C2/c* (No. 15)	*1363(2)*
140	15.42(1)	14.5(1)	6.62(1)	–	*Pnam* (No. 62)	1481(1)
140	*17.54(2)*	*12.09(2)*	*6.65(2)*	*105.2(2)*	*C2/c* (No. 15)	*1361(2)*
120	15.41(1)	14.48(1)	6.62(1)	–	*Pnam* (No. 62)	1477(1)
120	*17.53(2)*	*12.08(2)*	*6.64(2)*	*105.1(2)*	*C2/c* (No. 15)	*1360(2)*
100	15.39(1)	14.45(1)	6.62(1)	–	*Pnam* (No. 62)	1471(1)
100	*17.52(2)*	*12.08(2)*	*6.64(2)*	*105.0(2)*	*C2/c* (No. 15)	*1358(2)*

[a] For temperatures between 160 and 100 K, mixtures of the orthorhombic and monoclinic cells were present; data for the latter are shown in italics.

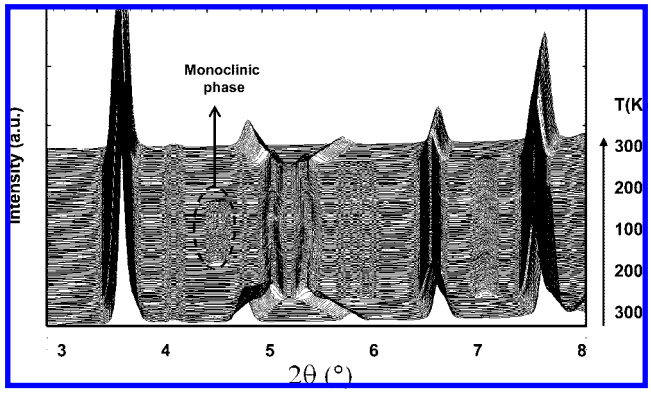

Figure 10. Evolution of the XRD patterns (λ = 0.7 Å) of MIL-53(Al) filled with *n*-hexane ($p/p°$ = 0.6 at 313 K) as a function of temperature.

a capillary containing a powdered sample of MIL-53(Al) filled with *n*-hexane at a partial pressure of $p/p°$ = 0.6 at 303 K was analyzed in situ using X-ray synchrotron radiation at the Swiss−Norwegian beamline at ESRF. The temperature was decreased from 300 to 100 K using a cooling system and finally set back to 300 K (step: 10 °C/scan). The cell parameters as a function of the temperature were obtained using the Dicvolgv software (see Table 1).

First, the symmetry, which was previously determined to be orthorhombic *Imcm* (No. 74) during the first ex situ experiments, turned out to be different than expected [*Pnam* (No. 62)]. This is probably due to the aging in time of the sample.

Second, as expected, a slight increase in the cell volume occurs as the temperature is initially decreased from 300 K to 220 K, in agreement with an increase in the partial pressure. Interestingly, the cell volume stabilizes and then finally decreases significantly, from 1488 to 1471 Å^3, as *T* further decreases to 100 K.

Third, some additional peaks appear at $2\theta \approx 4.5$ and 8.7° (see Figure 10), and the overall pattern cannot be assigned in either the initial orthorhombic cell or another monoclinic or orthorhombic space group, indicating that a second phase has appeared. Despite the difficulty in unambiguously finding the cell parameters and space group of the unknown phase, a monoclinic cell [*C2/c* (No. 15)] having a volume close to 1350 Å^3 is proposed (Table 1). A pattern match including the two phases, i.e., orthorhombic *Pnam*

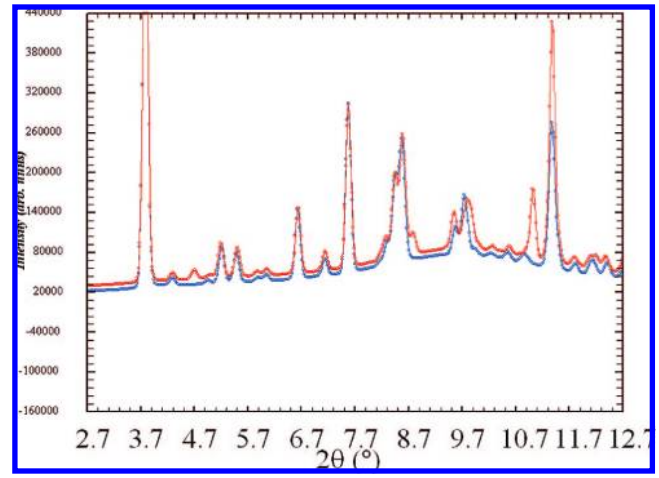

Figure 11. Comparison between the XRD patterns (synchrotron radiation, λ = 0.7 Å) indexed in the orthorhombic symmetry and the monoclinic one.

and monoclinic *C2/c* cells, was successfully performed, validating this hypothesis (see Figure 11).

The cell volume and parameters of this intermediate monoclinic cell are very close to those of the narrow pore form shown by ex situ XRD using the sample containing *n*-hexane at a partial pressure of $p/p°$ = 0.1 at 303 K (Table 1).

These results are in agreement with a decrease in hexane loading capacity at low temperature for MIL-53(Al). This can be explained by the breathing behavior of MIL-53. Brown and co-workers[37b] have shown that a dehydrated MIL-53(Al) sample can be stabilized in its narrow-pore form upon cooling to 77 K; its pores open upon heating, and when it is cooled, a closure of the pores occurs at low temperature (<200 K).

Thus, a competition between the traditional adsorption laws (increase of the loading capacity upon cooling) and the thermodynamics of breathing (closure of the pores with decreasing temperature) is the origin of the unusual thermal evolution of the loading capacity of MIL-53.

Conclusion

This initial study paves the way for the comprehensive use of flexible MOF structures for novel adsorption or separation processes involving vapors. The adsorption of species as simple as model linear alkanes in MIL-53(Al, Cr) is not straightforward, as different sorption behaviors can be observed depending on the nature of the metal centers. Several features arise from this study. First, the microporous MIL-53 exhibits strong affinities and large adsorption capacities for alkanes. Second, there is a clear influence of the alkyl chain length on the shape of the adsorption curves, suggesting important conformational effects from guest species in addition to a breathing of the structure for long-chain alkanes. Furthermore, the pressures at which the substeps occur depend on the nature of the metal (Al, Cr). In both cases (chain length, metal), as the pressure logarithm can be related to free energy, this confirms that energetic considerations related to the interaction that occurs between the *n*-alkane species and the MOF frameworks can be the origin of these differences.

The kinetics of adsorption was investigated and revealed the presence of several regimes influenced by both the alkyl chain length and the temperature. Finally, a very unusual temperature dependence of the loading capacity was observed, which might

be due to a competition between standard adsorption thermodynamics and the temperature-dependent increase in pore opening of the MIL-53 solids. Further studies are underway to gain a deeper understanding of the use of flexible MOFs for the adsorption of hydrocarbons.

Acknowledgment. The authors thank Dr. Nathalie Guillou (Versailles) for her help with the XRD measurements. The authors are also indebted to the ESRF in Grenoble for providing beamtime and the help of their staff during and after the experiments. The authors are also indebted to ANR (BLAN07-1_203677 SAFHS).

Supporting Information Available: Kinetics of sorption of *n*-hexane, *n*-heptane, *n*-octane, and *n*-nonane at zero coverage (first sorption equilibrium) (Figure S1). This material is available free of charge via the Internet at http://pubs.acs.org.

JA8039579